Chemosphere 277 (2021) 130280

Contents lists available at ScienceDirect

Chemosphere

journal homepage: www.elsevier.com/locate/chemosphere

Tar steam reforming for synthesis gas production over Ni-based on ceria/zirconia and $La_{0.3}Sr_{0.7}Co_{0.7}Fe_{0.3}O_3$ in a packed-bed reactor

Chalempol Khajonvittayakul [a], Vut Tongnan [a], Netiwat Namo [b], Chutamat Phonbubpha [b], Navadol Laosiripojana [c], Matthew Hartley [b], Unalome Wetwatana Hartley [a, c, *]

[a] Chemical and Process Engineering, The Sirindhorn International Thai-German Graduate School of Engineering (TGGS), King Mongkut's University of Technology North Bangkok, Bangkok, 10800, Thailand
[b] Department of Chemical Engineering, Faculty of Engineering, King Mongkut's University of Technology North Bangkok, 10800, Thailand
[c] Joint Graduate School of Energy and Environment (JGSEE), King Mongkut's University of Technology Thonburi, Bangkok, 10140, Thailand

HIGHLIGHTS

- 5% nickel on $Ce_{0.9}Zr_{0.1}O_2$ gives the best performance.
- Optimum reaction temperature of 700 °C.
- Ceria/zirconia showed better result compared to the perovskite.

ARTICLE INFO

Article history:
Received 27 October 2020
Received in revised form
27 February 2021
Accepted 7 March 2021
Available online 23 March 2021

Handling Editor: Derek Muir

Keywords:
Catalytic steam reforming
Coke deposition
Nickel base metal oxide
Synthesis gas production

ABSTRACT

In this work, NiO level was varied from 5 to 40% whereas $Ce_xZr_{1-x}O_2$ (x = 0.5, 0.7 and 0.9) (CZO) and $La_{0.3}Sr_{0.7}Co_{0.7}Fe_{0.3}O_3$ (LSCF) were chosen as two different kinds of support. Regardless the type of support, the surface NiO (at 40%) was completely reduced at 600 °C, giving the amount of activated Ni at 8950 μmol/g_{cat}. The reducibility of the updoped LSCF was found to be much better than that of the undoped CZO, evidenced by the H_2-TPR of the both materials at 600 °C where the oxygen storage capacity (OSC) of LSCF and CZO was determined at 4273 and 307 μmol/g_{cat}, respectively. In contrast, the OSC of 40%Ni-CZO (where x = 0.7, 0.9) was found to be higher than that of the LSCF, implying that the addition of Ni more enhanced both electronic defect and oxygen mobility in CZO than in LSCF, according to the H_2-TPR results. Coke resistant of CZO is presumable more satisfying than that of LSCF, thus, the longer lifespan of the CZO catalyst system is expected. The catalytic performance of 40%Ni-CZO (x = 0.9) was however comparable with 40%Ni-LSCF as they accommodate the same number of active sites. The slightly better catalytic performance of the 40%Ni-CZO (x = 0.9) could be due to its smaller crystallite size (CZO = 26.83, LSCF = 35.73), rendering more access for the relative gaseous reactants. The best catalyst amongst all was 5%Ni-CZO (x = 0.9), giving 89% toluene conversion, 46% H_2 yield, 71% CO selectivity, and 25% CO_2 selectivity at optimum reaction temperature of 700 °C.

© 2021 Elsevier Ltd. All rights reserved.

1. Introduction

Thailand 4.0 has launched a new concept of BCG model where bio-economy, circular economy and green economy are integrated to encourage the innovation-based economy. Biomass is one of classical energy sources that meets the nation's policy, only if it can be environmentally-friendly handled. Green energy, either in the form of (1) combustible mixed gas or (2) syngas (for power generation), from biomass are mainly derived by gasification process at relatively high temperature, up to 700 °C. While the desired gaseous products can be obtained via this green gasification process, however, tar is one of the most unwanted by-products as it can cause various complexity in the system i.e. clogging, corrosion and erosion in the piping system and equipment. Besides, the presence of tar will decrease heat transfer efficiency in the gasifier and its associated units, yet reduce overall thermal efficiency of the process (Guan et al., 2016; Kuchonthara et al., 2012). The removal of tar

* Corresponding author. Chemical and Process Engineering, The Sirindhorn International Thai-German Graduate School of Engineering (TGGS), King Mongkut's University of Technology North Bangkok, Bangkok, 10800, Thailand.
E-mail address: unalome.w.cpe@tggs-bangkok.org (U.W. Hartley).

https://doi.org/10.1016/j.chemosphere.2021.130280
0045-6535/© 2021 Elsevier Ltd. All rights reserved.

from the process, for other possible uses is therefore crucial. Tar can be removed by various methods, for instance, filtration and water scrubber, where the rate of removal is considerably low (Nakamura et al., 2016). More advanced abatement methods include thermal cracking, catalytic cracking, catalytic steam reforming, dry reforming or carbon formation have been reported to remove tar as high as 98–99% (Milne et al., 1998; Vivanpatarakij and Assabumrungrat, 2013). Primary and secondary methods for tar abatement for the gasification process have been studied in recent decades. In the primary methods, tar will be removed in the gasifier whereas the secondary methods are when tar is eliminated in a separated unit after the gasifier, which is the selected method in this research. Catalyst plays a big part in tar steam reforming. Good catalyst selection can reduce the reaction temperature while increase the process's efficiency. A number of catalysts had been studied and developed for the tar removal such as dolomite, magnesites, and zeolites. Ni-based metal oxide catalysts and novel metal catalysts (Ashok and Kawi, 2013; Han and Kim, 2008; Li et al., 2009a, 2009b; Liu et al., 2020a, b; Soomro et al., 2018; Świerczyński et al., 2007). The catalytic performance of such works had been compared and tabulated in Table 2. The studied metal oxides include ceria/zirconia and perovskites due to its high oxygen vacancy and mobility. Nickel-based catalysts have been widely applied for the removal and transformation of tar in petrochemical industry. Our previous studies revealed that nickel-based catalysts have been proven to be relatively more effective in removing heavy tars, showing high activity, which could substantially assist in reforming of biomass tar (Hartley et al., 2015; Kangsadan et al., 2015; Wetwatana et al., 2010). However, the major problem that is associated with nickel-based catalyst is the coke deposition and/or metal sintering (Baker et al., 1987; Bampenrat et al., 2010; Garcia et al., 2000), leading to deactivation of the catalysts and the reduction of activity in a long-term operation. Dayton et al. proposed to solve such problem by increasing surface oxygen's mobility and reducing Ni's particle size (Dayton, 2002). Cerium oxide (CeO_2) is well-known to be a good support for nickel due to its high oxygen vacancy and high redox properties in which it helps to combust the coke formation. The addition of zirconium in CeO_2 was found to improve the catalyst system's performance as it is able to combust coke and simultaneously provides high thermal stability (Łamacz et al., 2011; Laosiripojana and Assabumrungrat, 2005, 2006). Nickel based catalyst on cerium-zirconium oxide support has been utilized extensively in reforming reactions, water gas shift and partial oxidation of hydrocarbons (Alvarez-Galvan et al., 2019; Jang et al., 2019; Łamacz et al., 2019) (Bampenrat et al., 2010; Chen et al., 2008; Pengpanich et al., 2004). Apart from the ceria/zirconia materials in which they are well-known for their high oxygen storage capacity, the Perovskites (ABO_3) are also becoming more attractive in the past decade for the same reason. In addition, the perovskites tend to have high lattice oxygen conductivity (e.g. $LaAlO_3$ and $La_{0.7}Sr_{0.3}AlO_3$), leading to high activity and high resistance to carbon formation (Higo et al., 2015; Mukai et al., 2013; Sekine et al., 2013; Urasaki et al., 2005). Amongst all the perovskites, $La_{0.3}Sr_{0.7}Co_{0.7}Fe_{0.3}O_3$ (LSCF3773) perovskite was found to be one of the most promising ones due to its redox properties and structures (Babiniec et al., 2015). This research investigated the catalytic performance of Ni-based catalysts on supports; i.e. LSCF3773 perovskite and cerium-zirconium oxide; for tar steam reforming. The effects of nickel content, molar ratio of cerium to zirconium, and operating temperature were investigated. The performance of the catalysts was evaluated in terms of conversion, selectivity, and yield.

2. Methodology

2.1. Catalyst preparation

2.1.1. Ni-doped $La_{0.3}Sr_{0.7}Co_{0.7}Fe_{0.3}O_3$

LSCF3773 was prepared via EDTA-citrate complex method (Hartley et al., 2018; Khajonvittayakul et al., 2019; Khamhangdatepon et al., 2020) from relevant nitrate (NO_3) precursors which are 0.6215 g of $La(NO_3)_3 \cdot 6H_2O$ (Sigma Aldrich, 99.0%), 0.7088 g of $Sr(NO_3)_2$ (Himedia, 98.0%), 0.5799 g of $Fe(NO_3)_3 \cdot 9H_2O$ (Univar, 99.0%), and 0.9747 g of $Co(NO_3)_2 \cdot 9H_2O$ (Carlo ERBA, 99.0%). The precursors were dissolved in 200 ml distilled water and stirred continuously until a transparent aqueous solution was acquired. The pH of the solution was maintained at 7–8 by adding EDTA-NH_4OH solution drop-wise. Ethylene glycol was afterwards mixed into the solution while stirring. The solution was heated up to 80–90 °C until becoming clear dark brownish gel. The resulting gel was dried in a vacuum oven at 180 °C overnight before being calcined in a flowing air at 1000 °C for 24 h, at 10 °C/min of heating rate, to successfully form high purity LSCF3773. Ni was doped on LSCF3773 using wet impregnation method. The synthesized LSCF3773 powder was added into a nickel nitrate aqueous solution which was stirred until the solution became homogeneous. In order to produce gelation, $(NH_4)_2CO_3$ aqueous solution was dropped into the homogeneous solution using a syringe pump at 5 ml/min flow rate, maintaining its pH at 8. The resulting mixture was heated up until volatile solvent was evaporated at 80–90 °C and then dried at 150 °C overnight. The greenish-black powder was mashed, and calcined at 900 °C with a heating rate at 10 °C/min for 12 h in a flowing air.

2.1.2. Ni-doped $Ce_xZr_{1-x}O_2$ catalysts

Different level of Ni was doped on $Ce_xZr_{1-x}O_2$ (x = 0.9, 0.7, and 0.5) at 5, 10, 20, and 40% by weight. The support, $Ce_xZr_{1-x}O_2$ (CZO(x:1-x)), was prepared by using one-pot hydrolysis method

Table 1
Oxygen release calculated from H2 uptake via H_2-TPR (from Figs. 3 and 4).

Catalyst	Oxygen release (μmol/g_{cat})						
	Total				Reduced at 600 °C		
	All	Surface	Bulk	Active phase[a]	All	Activated active phase[b]	Support[b]
NiO	22,376	n/a	n/a	n/a	20,671	n/a	n/a
LSCF	8393	2469	5924	n/a	4273	n/a	n/a
Ni-LSCF	12,876	1984	10,892	8950	9232	8250	964
CZO	1286	466	820	n/a	307	n/a	n/a
Ni-CZO (1:1)	13,686	13,686	n/a	8950	8250	8250	0
Ni-CZO (7:1)	12,008	12,008	n/a	8950	9850	8250	1582
Ni-CZO (9:1)	11,633	11,633	n/a	8950	11,470	8250	3202

[a] Calculated based on 40% of pure NiO reduction.
[b] Normalized.

Table 2
The comparison of 40%Ni/$Ce_{0.9}Zr_{0.1}O_2$ and 40%Ni/LSCF3773 at 700 °C, S/C ratio is 2, holding time as 1.30 h, and the amount of catalyst 0.5 g.

Type of Catalytic	Toluene Conversion (%)	Selectivity (%)			H_2 yield (%)	H_2:CO ratio
		CO	CO_2	CH_4		
40%Ni/$Ce_{0.9}Zr_{0.1}O_2$	80	74	24	2	55	2.42
40%Ni/LSCF3773	73	73	26	1	46	2.18

where the detailed procedure was described elsewhere (Ngoenthong et al., 2019). In brief, all metal nitrate precursors (1.7077 g of $Ce(NO_3)_3 \cdot 6H_2O$ and 0.2392 g of $ZrO(NO_3)_2$. xH_2O for x = 0.9) were mixed with 0.1 M cetyltrimethyl ammonium bromide (CTAB). The pH was adjusted to 11 with NaOH and washed with DI water. Then, the precipitate was dried at 120 °C overnight and calcined at 700 °C with 2 °C/min of heating rate for 3 h in air. After that, the obtained solid was mixed into $(NH_4)_2CO_3$ aqueous solution. The same step in Ni-doped on LSCF preparation of evaporation, drying at 120 °C, and calcination at 900 °C with 10 °C/min of heating rate for 12 h in air were applied.

2.2. Characterizations

The prepared catalysts were characterized using X-Ray diffraction technique (XRD), hydrogen temperature programmed reduction (H_2-TPR), and oxygen temperature programmed oxidation (O_2-TPO). The crystallinity, crystallite size (calculated using Scherrer equation) and structure of the prepared catalysts were identified by XRD technique using a diffractometer (Rigaku TTRAX III), Cu Kα radiation, λ = 1.5418 Å in a range of 30° < 2θ < 80° with a scanning step of 0.01°. The temperature programmed-reduction and oxidation were both carried out to define the catalyst's reducibility, appropriate reduction temperature of each catalyst (in-situ activation temperature before use) and the quantity of the carbon deposition. During both temperature programmed techniques, the catalysts were packed in a small tubular reactor (i.d. = 13 mm). The reactive mixed gases; i.e. 5%H_2/Ar for H_2-TPR and 2%O_2/Ar for O_2-TPO; were introduced into the reactor, in which the catalyst was packed, at a flow rate of 100 ml/min. The temperature was afterwards increased at 5 °C/min from 25 to 950 °C. The consumption of the reactant and the formation of the product gases were measured by real-time quadrupole mass spectrometer gas analyser (MS) as a function of interested gases and the transient temperature.

2.3. Catalytic performance assessment

A lab-scale experimental system was designed and set up, as shown in Fig. 1, for catalytic tar steam reforming. Toluene was used as a tar model (Guan et al., 2016; Han and Kim, 2008). The catalyst powder was pelletized, crushed and sieved to 180–212 μm in size before being placed in a middle of quartz tubular reactor (i.d. = 13 mm, length of bed = 1000 mm). Type K thermocouple was inserted inside, nearest to the catalyst's bed. The catalysts were activated by exposing to 100 ml/min of 10% H_2/Ar, which was held at 600 °C for 5 h. After completion of the reduction process, the reactor was cool down to ambient temperature and was afterwards flushed by Ar, until H_2 concentration was untraceable. The reactive gases i.e. toluene and water, were supplied using vaporizers and mass flow controllers. Steam to carbon molar ratio of the feed stream was kept constant at 2:1 for all experiments (Li et al., 2017; Sordi et al., 2009). Total flow rate was maintained at 100 ml/min using Ar as a balancing gas. The operating temperature was varied from 600 to 800 °C under atmospheric pressure. The measurement was performed after 1 h reaction time. The effluent gases were periodically analyzed using a Shimadzu GC-2014ATP, equipped with a thermal conductivity detector (TCD).

Toluene conversion (X_{C7H8}), selectivity of carbon containing products (S_i), and the hydrogen yield (Y_{H2}) were calculated as follows:

$$X_{C_7H_8}\ (\%) = \frac{F_{CO_{out}} + F_{CO_{2out}} + F_{CH_{4out}}}{7F_{C_7H_8\ in}} \text{x } 100 \quad (1)$$

$$S_{CO}\ (\%) = \frac{F_{CO_{out}}}{F_{CO_{out}} + F_{CO_{2out}} + F_{CH_{4out}}} \text{x } 100 \quad (2)$$

$$S_{CO_2}\ (\%) = \frac{F_{CO_{2out}}}{F_{CO_{out}} + F_{CO_{2out}} + F_{CH_{4out}}} \text{x } 100 \quad (3)$$

$$S_{CH_4}(\%) = \frac{F_{CH_{4out}}}{F_{CO_{out}} + F_{CO_{2out}} + F_{CH_{4out}}} \text{x } 100 \quad (4)$$

$$Y_{H_2}\ (\%) = \frac{F_{H_{2out}}}{18F_{C_7H_8\ in}} \text{x } 100 \quad (5)$$

where F_{C7H8in} is an inlet molar flow rate (mmol/min). F_{COout}, F_{CO2out}, F_{CH4out}, and F_{H2out} are outlet molar flow rate of carbon monoxide, carbon dioxide, methane, and hydrogen (mmol/min), respectively (Li et al., 2009a; Sekine et al., 2013).

3. Result and discussion

3.1. Crystallographic structure by X-Ray diffraction technique (XRD)

Fig. 2 illustrates diffractograms of the prepared catalysts (40% Ni-doped LSCF3773 and $Ce_xZe_{1-x}O_2$ at x = 0.5, 0.7 and 0.9) after calcined at 900 °C. The cubic crystal structure of NiO (ICDD card No.03-065-5745) was presented as a minor crystalline phase in all catalysts, at two theta angle of 37.3°, 43.4°, 62.9°, and 75.5°, which were corresponded to (111), (200), (220), and (311) planes) (Ding et al., 2008; Nie et al., 2017). The perovskite phase of LSCF3773 can be seen as expected in Fig. 2(d), which was presented at 2θ = 23.2°, 33.0°, 40.7°, 47.4°, 53.94°, 59.0°, 69.2°, and 78.8°, whereas ceria-zirconia phase, possessing fluorite structure, was shown at 2θ = 28.5°, 33.2°, 47.6°, 56.5°, 59.2°, and 69.4°, agreeing with previous works reported by (Khajonvittayakul et al., 2019) and (Liu, 2018), respectively. In addition, the solely separated peaks of NiO from major crystalline phases; i.e. LSCF3773 and ceria-zirconia; indicated that the major crystalline phases were not interfere by the addition of NiO. From the diffractograms, the broader the peaks are, the smaller the crystalline size become, according to the Scherrer's equation (Monshi et al., 2012). The crystallite size of NiO in $Ce_{0.5}Zr_{0.5}O_2$ (a), $Ce_{0.7}Zr_{0.3}O_2$ (b), $Ce_{0.9}Zr_{0.1}O_2$ (c) and LSCF3773 (d) was calculated at 10.73, 13.54, 26.83, and 35.73, respectively, agreeing with the comparison of the diffractogram appearance. It was observed that the crystallite size is decreased when the ratio of Ce/Zr is decreased, possibly due to the larger ionic radius of Ce^{4+} (0.97 A), compared to that of Zr^{4+} (0.84 A) (Liu, 2018). The smaller crystallite size of the NiO is believed to have a positive influence on its catalytic performance towards the tar steam reforming reaction.

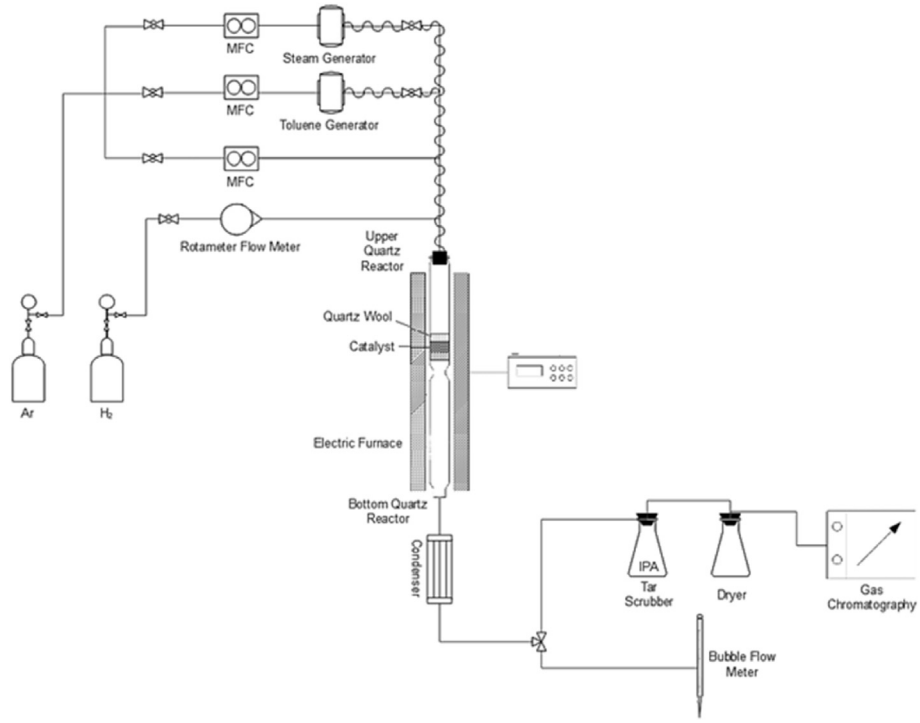

Fig. 1. Schematic diagram for catalytic tar steam reforming system.

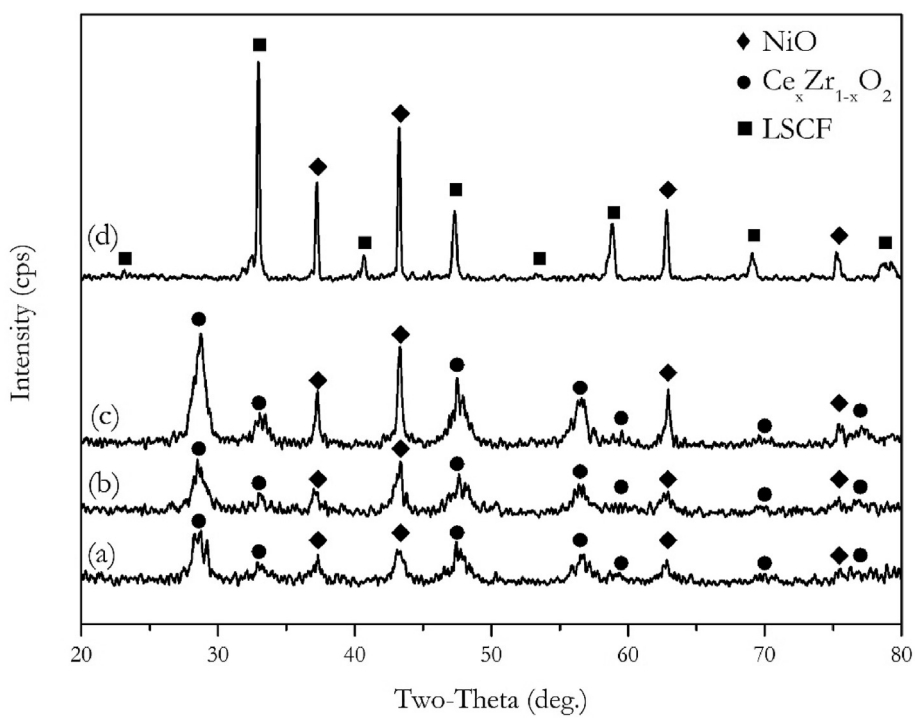

Fig. 2. XRD diffractograms pattern of 40%Ni dope on supports: (a) $Ce_{0.5}Zr_{0.5}O_2$, (b) $Ce_{0.7}Zr_{0.3}O_2$, (c) $Ce_{0.9}Zr_{0.1}O_2$, and (d) $La_{0.3}Sr_{0.7}Co_{0.7}Fe_{0.3}O_3$.

3.2. Reducibility by hydrogen temperature programmed reduction (H_2-TPR)

The reducibility of the prepared 40%Ni/$La_{0.3}Sr_{0.7}Co_{0.7}Fe_{0.3}O_3$ catalysts was characterized by exposing to 5%H_2/Ar while the H_2 consumption was measured with linear temperature transient. The result was demonstrated in Fig. 3. TPR profile of NiO presented two main reduction peaks centred at 395 and 500 °C. The low and high temperature reduction peaks are ascribed to the reduction of Ni^{3+} ions → Ni^{2+} ions and Ni^{2+} ions → Ni^0 ions, respectively (Bai, 2013). On the other hand, the TPR profile of the un-doped LSCF showed four reduction peaks at 360, 560, 745 and 860 °C. The first peak is

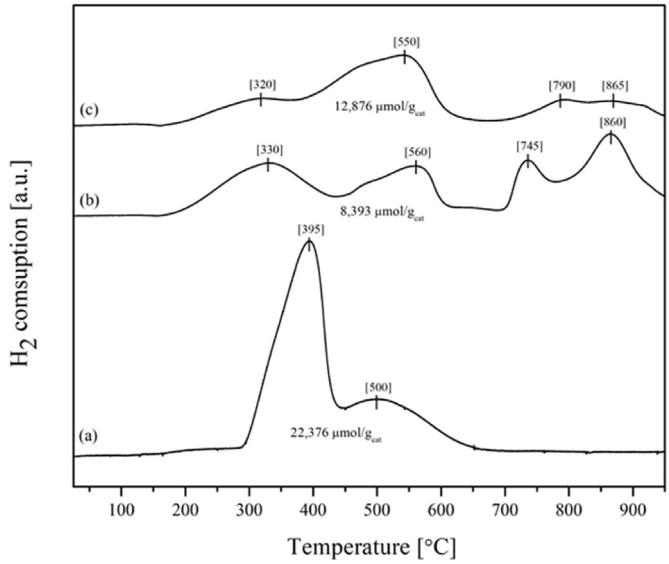

Fig. 3. H_2-TPR profiles of synthesized catalysts: (a) NiO, (b) $La_{0.3}Sr_{0.7}Co_{0.7}Fe_{0.3}O_3$, and (c) 40%Ni/$La_{0.3}Sr_{0.7}Co_{0.7}Fe_{0.3}O_3$.

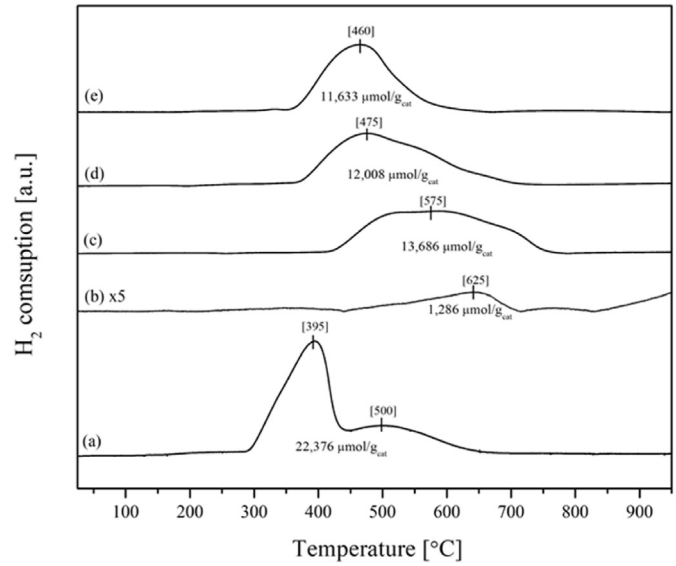

Fig. 4. H_2-TPR profiles of synthesized catalysts: (a) NiO, (b) $Ce_{0.9}Zr_{0.1}O_2$, (c) 40%Ni/$Ce_{0.5}Zr_{0.5}O_2$, (d) 40%Ni/$Ce_{0.7}Zr_{0.3}O_2$, and (e) 40%Ni/$Ce_{0.9}Zr_{0.1}O_2$.

responsible for the surface reduction and the rest three are due to the bulk reduction where Co^{3+}/Fe^{4+}, Fe^{5+} ions → Co^{2+}/Fe^{3+} ions → Co^0/Fe^{2+} ions → Co and Fe (Khajonvittayakul et al., 2019). Similarly, the 40%NiO doped LSCF3773 showed almost identical TPR peaks. However, some of the bulk reduction peaks were found to significantly shift to the higher temperatures (from 745 to 790 °C). This could be due to the strong interaction between Ni and the LSCF, causing the reduction of the catalyst more difficult. From the results, it was observed that the surface reduction of all catalysts were completed at 600 °C, thus, this temperature was chosen to be the reduction temperature of all the LSCF catalysts before use as the reaction is tended to occur at the surface level rather than bulk, especially if the kinetic rate is relatively high. In addition, the surface NiO was completely reduced at 600 °C except for those ones that were segregated into the bulk solid, due to the high degree of doping (40%). However, it was believed that, at this temperature, all the NiO at the surface should be completely reduced, while the surface LSCF were also partly reduced too. Similarly, H_2-TPR profiles of the 40%NiO doped on $Ce_xZr_{1-x}O_2$ (x = 0.5, 0.7, and 0.9), the undoped $Ce_{0.9}Zr_{0.1}O_2$ and the pure NiO were as well presented in Fig. 4. The doped catalysts were found to have higher reducibility compared to the un-doped one, evidenced by their relatively lower reduction temperatures. The Zr content was found to have quite an influence on the overall catalyst system's reducibility. Comparing between the doped-catalysts, the higher the Zr level is, the higher the reduction temperature become. This was the result of the stronger bonding interaction between NiO and the mixed support (Nie et al., 2017). The support itself without NiO doping ($Ce_{0.9}Zr_{0.1}O2$) was found to be reducible (reduction of Ce^{4+} to Ce^{3+} (Sun et al., 2019) seen as one low-amplitude broad peak) at 625 °C, the highest temperature among all, giving the lowest H_2 uptake at 1286 μmol/g_{cat}. Effect of Zr substitution is believed to solely enhance the formation of structural defects ($Ce_xZr_{1-x}O_{2-\delta}$, where δ = oxygen defect) which is expected to play an important role in reduction/oxidation reaction (Biswas and Kunzru, 2007; Córdoba and Martínez-Hernández, 2015; Ngoenthong et al., 2019; Trovarelli et al., 1997), while not participating in the reduction/oxidation process itself. The degree of reduction of 40%Ni/$Ce_xZr_{1-x}O_2$ catalyst was estimated in term of H_2 consumption (μmol/g_{cat}). The total H_2 uptakes of 40%Ni/$Ce_{0.9}Zr_{0.1}O_2$, 40%Ni/$Ce_{0.7}Zr_{0.3}O_2$, and 40%Ni/$Ce_{0.5}Zr_{0.5}O_2$ were 11,633, 12,008, and 13,686 μmol/g_{cat}, respectively. Thus, the suitable reduction temperature for the catalyst's activation is predicted to be varied from 520 to 600 °C. Kinetic rate of H_2 uptakes on 40%Ni/$Ce_{0.9}Zr_{0.1}O_2$ was found to be faster than that of 40%Ni/$Ce_{0.7}Zr_{0.3}O_2$ and 40%Ni/$Ce_{0.5}Zr_{0.5}O_2$. Whereas the 40%Ni/$Ce_{0.9}Zr_{0.1}O_2$ possesses the highest oxygen mobility as it took the shortest reduction time and consumed hydrogen most rapidly. For this reason, 40%Ni/$Ce_{0.9}Zr_{0.1}O_2$ catalyst is believed to be the best amongst all the studied catalysts for converting tar to synthesis gas.

To clarify the meaning of H_2 uptake, its amount presumably represents amount of the oxygen released either from surface and/or from bulk of the catalyst sample, as well as either from the active phase (NiO) and/or from the supports (40%Ni/$La_{0.3}Sr_{0.7}Co_{0.7}Fe_{0.3}O_3$ and 40%Ni/$Ce_{0.9}Zr_{0.1}O_2$). Since the complete reduction of NiO was assured at 600 °C as explained previously, its amount of oxygen release was then theoretically calculated to 8950 μmol/g_{cat}. Thus, the rest of the oxygen release was presumably the oxygen lattice, which was released from the supports. Table 1 summarizes amount of the oxygen release from active phase and the supports in comparison, as well as the oxygen release by the surface and bulk reduction of each catalyst.

When reduced at 600 °C, the amount of activated Ni was estimated at 8250 μmol/g_{cat} whereas the active OSC of 40%Ni/LSCF3773, 40%Ni/$Ce_{0.5}Zr_{0.5}O_2$, 40%Ni/$Ce_{0.7}Zr_{0.3}O_2$ and 40%Ni/$Ce_{0.9}Zr_{0.1}O_2$ was calculated at 964, 1582 and 3202 μmol/g_{cat}, respectively. This implied that the reactivity of all the catalysts, due to the reactive Ni, should be more or less the same, however, the ability to combust coke deposition will be different, according to the level of OSC the support possesses. In this case, the ceria-zirconia catalyst system should be able to eliminate coke formation (via equation (16)) better than the LSCF.

3.3. *Effect of stoichiometric proportion of $Ce_xZr_{1-x}O_2$ catalyst (x = 0.5, 0.7, and 0.9)*

Fig. 5 presented catalytic performance of $Ce_xZr_{1-x}O_2$ catalysts with different stoichiometric ratio of Ce/Zr, where x = 0.5, 0.7, and 0.9, at operating temperature ranging from 600 to 750 °C.

It was obvious that at the higher operating temperatures, the

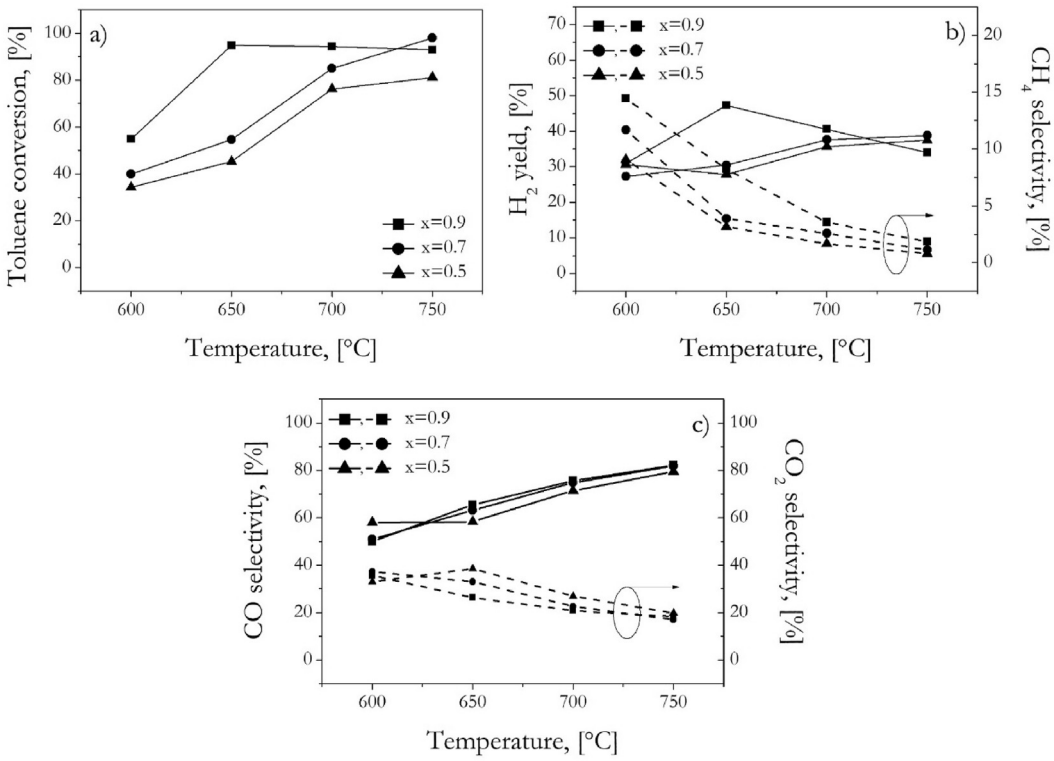

Fig. 5. Effect of (■) 40% Ni/$Ce_{0.9}Zr_{0.1}O_2$; (•) 40% Ni/$Ce_{0.7}Zr_{0.3}O_2$; (▲) 40% Ni/$Ce_{0.5}Zr_{0.5}O_2$ on a) the conversion of C_7H_8, b) the selectivity of CH_4 and yield of H_2, and c) the selectivity of CO and CO_2. Reaction condition: S/C ratio is 2 and holding time as 1.30 h for each temperature and the amount of catalyst 2.5 g.

toluene conversion, H_2 yield and CO selectivity were increased, whereas the CH_4 and CO_2 selectivity were decreased. The reaction pathways could be presumably described as shown in the following equations (Oemar, 2014) and (Łamacz et al., 2011):

Surface water dissociation (where O^* represents oxygen vacancy):

$$H_2O + * \rightarrow O^* + H_2 \quad (6)$$

Decomposition of toluene on Ni and maybe the reduced supports:

$$C_7H_8 + 2Ni \rightarrow C_6H_6 \cdot Ni + CH_2 \cdot Ni \quad (7)$$

$$C_6H_6 + 2Ni \rightarrow 3C_2H_2 \cdot Ni \quad (8)$$

C2 species reacting with O^* into aldehyde species:

$$C_2H_2 \cdot Ni + O^* \rightarrow C_2H_2O \cdot Ni + * \quad (9)$$

$$C_2H_2O \cdot Ni + Ni \rightarrow CH_2O \cdot Ni + C \cdot Ni \quad (10)$$

$$CH_2 \cdot Ni + O^* \rightarrow CH_2O \cdot Ni + * \quad (11)$$

$$CH_2O \cdot Ni + Ni \rightarrow CHO \cdot Ni + H \cdot Ni \quad (12)$$

Decomposition of aldehyde to the expected final products; H_2, CO and CO_2:

$$CHO \cdot Ni + Ni \rightarrow CO \cdot Ni + H \cdot Ni \quad (13)$$

$$CO \cdot Ni + O^* \rightarrow CO_2^* + Ni \quad (14)$$

$$C \cdot Ni + O^* \rightarrow CO + Ni + * \quad (15)$$

$$C \cdot Ni + CO_2^* \rightarrow 2CO + Ni + * \quad (16)$$

Methane formation and decomposition:

$$C \cdot Ni + 2H_2 \leftrightarrow CH_4 + Ni \quad (17)$$

Desorption of the final products:

$$2H \cdot Ni \rightarrow H_2 + 2Ni \quad (18)$$

$$CO \cdot Ni \rightarrow CO + Ni \quad (19)$$

$$CO_2^* \rightarrow CO_2 + * \quad (20)$$

From the previous observation (Fig. 5), CO_2 amount was decreased when CO formation was increased due to the conversion of CO_2 to CO; meaning that either the rate of eq. (16) is possibly higher than that of eq. (20) or the CO_2 was utilized further for methane dry reforming; at higher temperature. Besides, CH_4 was found to be decreased when the temperature was increased too, as a result of methane dry/methane reforming (Nam et al., 2018) (Sun et al., 2015), which normally occur at high temperature ranging from 700 to 1100 °C, and reverse water gas shift reaction. The $Ce_{0.9}Zr_{0.1}O_2$ shows the best performance among all.

3.4. Performance of 40%Ni/$Ce_{0.9}Zr_{0.1}O_2$ and 40%Ni/LSCF3773

The performance of $Ce_{0.9}Zr_{0.1}O_2$ and LSCF3773 catalysts was investigated at operating temperature of 700 °C, with Ni content of 40%. The results were compared in Table 2, which illustrates that the catalytic performance between the two catalysts are more or

less quite similar. However, 40%Ni/$Ce_{0.9}Zr_{0.1}O_2$ gave slightly higher catalytic performance; i.e. higher toluene conversion, higher yield of H_2 and CH_4, yet lower CO_2 selectivity; compared to that of the 40%Ni/LSCF3773, despite having less H2-uptake (according to the TPR result).

The results agreed with the previous observation where the complete NiO reduction was suggested. Thus, the number of active phase in both catalysts shall be comparable, corresponding to the catalytic performance of both catalysts reported in Table 2. However, the smaller crystallite size of NiO in the 40%Ni/$Ce_{0.9}Zr_{0.1}O_2$, was suspected to be responsible for its slightly higher catalytic performance, compared with that of the 40%Ni/LSCF3773. In addition, CO formation, considerably related to the ability to combust carbon of the supports (equation (15)), of both catalysts were similar, despite the fact that the OSC of the 40%Ni/$Ce_{0.9}Zr_{0.1}O_2$ (3202 μmol/g_{cat}) was reported to be around 3 times higher than that of the 40%Ni/LSCF3773 (964 μmol/g_{cat}), according to the interpreted data from Table 1. This implied that the amount of coke formation in both catalysts must be similar, thus, the OSC effect on the coke combustion cannot be compared in this case.

3.5. Effect of Ni content on the $Ce_{0.9}Zr_{0.1}O_2$ support

Fig. 6 illustrates the effect of Ni loading level on $Ce_{0.9}Zr_{0.1}O_2$ catalyst's system. Overall, 5% of Ni showed the best catalytic performance amongst all, offering toluene conversion of 90% and H_2 yield of 43%. Coke deposition formed by the use of 5%Ni, 10%Ni, 20% Ni and 40%Ni/$Ce_{0.9}Zr_{0.1}O_2$ was determined at 46,038 μmol/g_{cat}, 59,713 μmol/g_{cat}, 46,322 μmol/g_{cat} and 47,959 μmol/g_{cat}, respectively. When the same catalyst systems are being compared, the coke formation is expected to be higher if the reactivity is higher. Thus, it is not surprising if the 40%Ni/$Ce_{0.9}Zr_{0.1}O_2$ showed the least coke formation, according to its lowest reactivity/catalytic performance. However, 5%Ni/$Ce_{0.9}Zr_{0.1}O_2$ did not give the highest amount of coke formation, despite having the highest reactivity. This was possibly due to its surface OSC which is believed to be the highest as the lower percentage of Ni will sensibly leave the higher surface OSC, due to less chance of Ni particles agglomeration at the surface.

3.6. Effect of temperature on 5%Ni/$Ce_{0.9}Zr_{0.1}O_2$

Effect of operating temperature on the performance of 5%Ni/$Ce_{0.9}Zr_{0.1}O_2$ catalyst was investigated in a range of 650–800 °C and is shown in Fig. 7. When the temperature was increased, the toluene conversion was also increased. However, when the temperature was higher than 750 °C, the toluene conversion was found to be decreased, due to coke formation and sintering (Ashok et al, 2015, 2017). At the higher temperature, the syngas ratio was decreased as the H_2 yield did not significantly CO yield increased while that of H_2 remained constant. In this case, the optimal operating temperature was considered at 700 °C. At this temperature, the process will produce the syngas at the readily-utilized ratio (Hernández et al., 2017), around 2 of H_2 to CO. . From Fig. 7 (b), it can be seen that CO formation was favored at relatively high temperature, resulted by the endothermic reverse water gas shift reaction (Gao et al., 2015; Zhao et al., 2010. This phenomenon led to the drop in H2 yield during the same temperature range as it was consumed to react with CO2, and creating CO. At 700 °C, the toluene conversion, H2 yield, CO selectivity, CO2 selectivity and the syngas ratio was obtained at 89%, 46%, 71%, 25% and 2, respectively.

Our most promising catalyst, 5%Ni/$Ce_{0.9}Zr_{0.1}O_2$, was compared with other recent catalysts that have been developed recently, as

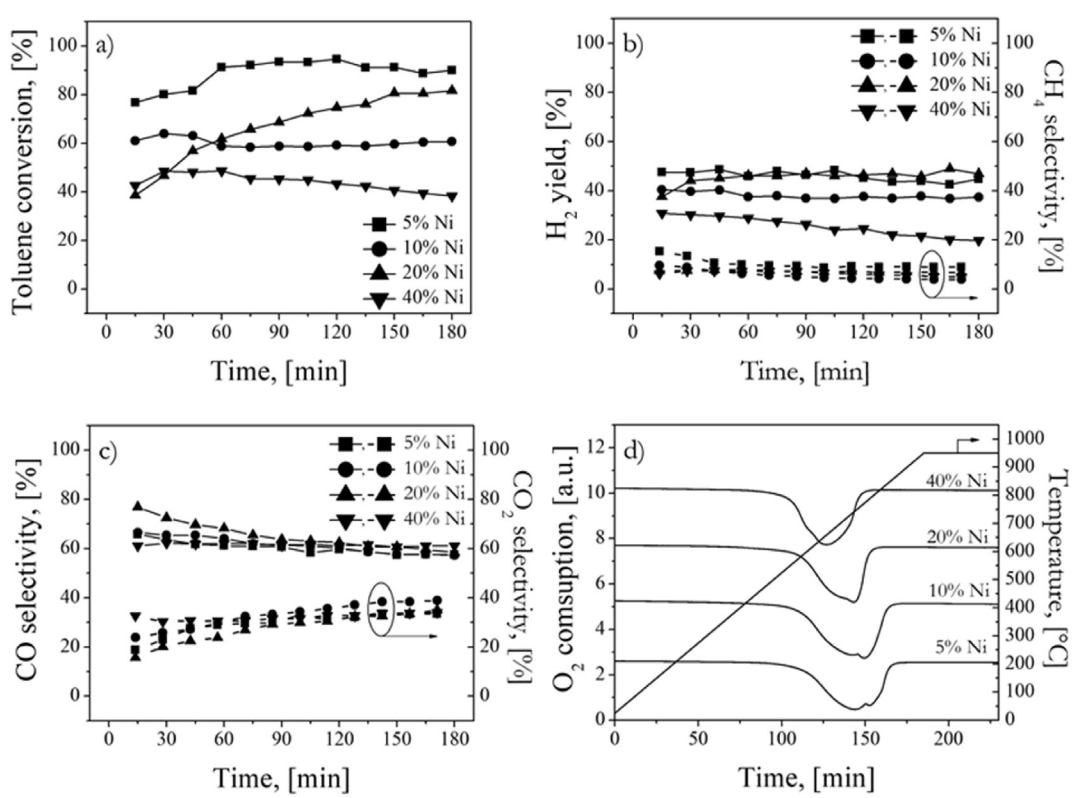

Fig. 6. Effect of (■) 5%Ni/$Ce_{0.9}Zr_{0.1}O_2$; (•) 10%Ni/$Ce_{0.9}Zr_{0.1}O_2$; (▲) 20%Ni/$Ce_{0.9}Zr_{0.1}O_2$; (▼) 40%Ni/$Ce_{0.9}Zr_{0.1}O_2$ on a) the conversion of C_7H_8, b) the yield of H_2 and selectivity of CH_4, c) the CO and CO_2 selectivity, and O_2-TPO result after reactivity test. Reaction condition: reaction temperature = 650 °C, holding time as 180 min, S/C ratio is 2, and the amount of catalyst 0.5 g.

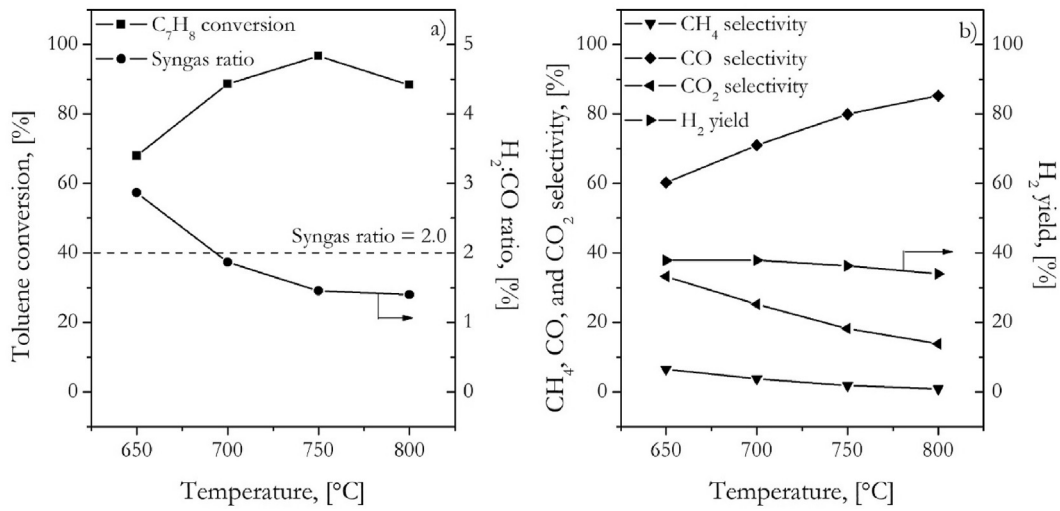

Fig. 7. Effect of temperature on 0.5 g of 5%Ni/$Ce_{0.9}Zr_{0.1}O_2$ where the feed reactant ratio S/C was fixed at 2; a) conversion of C_7H_8 and H_2:CO ratio and b) CH_4, CO, and CO_2 selectivity and yield of H_2.

shown in Table 3.

From Table 3, the catalyst from this work was found to provide the ratio of H_2 to CO closest to 2 (readily utilized further as intermediate in other chemical productions; i.e. methanol production, Fischer-Tropsch process; while the operating temperature was remained relatively low and industrially acceptable. The cost of catalyst also play a big part in catalyst selection criteria. The cost of ceria-zirconia catalyst is likely to be less than that of alkaline earth/transition metals contained in perovskites and/or mixed oxide compounds.

4. Conclusion

5%Ni/$Ce_{0.9}Zr_{0.1}O_2$ was found to be the most effective catalyst towards the tar reforming reaction; showing 89% toluene conversion, 46% H_2 yield, 71% CO selectivity, and 25% CO_2 selectivity, at

Table 3
Catalytic performance for steam reforming of toluene as a tar model compound over various catalysts.

Type of Catalysts	Reaction Conditions	Toluene Conversion (%)	Selectivity (%)			H_2 yield (%)	H_2:CO ratio	Reference
			CO	CO_2	CH_4			
10%Ni/CaO–Al_2O_3–CeO_2 Ca:Al:Ce = 1:0.8:0.2	T = 650 °C S/C = 3.4 W = 50 mg	100	35	63	3	–	4.2	Ashok and Kawi (2013)
5%Ni/$Ca_{12}Al_{14}O_{33}$	T = 700 °C S/C = 2.1 W = N/A	100	74	26	–	86	3.0	Li et al. (2009a)
Ni/ZSM-5	T = 650 °C S/C = 2.3 W = 0.6 g	100	59	41	–	84	4.2	Świerczyński et al. (2007)
0.1%Mg/9%Ni/$La_{0.7}Sr_{0.3}AlO_{3-\delta}$	T = 650 °C S/C = 2.0 W = 2 g	95	19	12	–	75	3.3	Zhang (2019)
Ni–Ca–Al(8:62:30)	T = 650 °C S/C = 1.0 W = 0.1 g	70	67	33	–	–	2.6	Ashok et al. (2015)
5%Ni/$La_{0.7}Sr_{0.3}AlO_{2.85}$	T = 600 °C S/C = 2.0 W = 1.65 g	73	41	51	7	–	–	Higo et al. (2015)
5%Ni/$La_{0.7}Sr_{0.3}AlO_{3-\delta}$	T = 600 °C S/C = 2.0 W = 25 mg	58	33	62	3	48	6.4	Mukai et al. (2013)
NiCoPhy@CeO_2	T = 700 °C S/C = 2.0 W = 0.1 g	80	50	50	–	–	4.5	Li (2019)
10%Ni/La_2O_3	T = 650 °C S/C = 1.0 W = 30 mg	36	49	50	1	–	3.8	Oemar (2015)
Ni/cordierite	T = 750 °C S/C = 2.0 W = N/A	75	52	48	–	–	3.8	Zhao et al. (2010)
5%Ni/$Ce_{0.9}Zr_{0.1}O_2$	T = 700 °C S/C = 2.0 W = 0.5 g	89	71	25	4	46	1.9	This work

700 °C.; with the syngas ratio of 2 which is considered to be readily utilized further in many chemical productions. The overall catalytic performance is comparable with the most recent developed catalysts, however, the techno-economic study can be carried out further to investigate whether the catalyst from this work is also cost effective. Despite possessing the best catalytic performance, the 5%CZO (9:1) has the lowest coke deposition, evidenced by O_2-TPD. This was possibly due to the fact that the amount of surface oxygen storage capacity (OSC) shall be higher, when the percent loading of NiO is lower, as the surface is free to accommodate the OSC, rather than the agglomerated NiO (especially at 40%) in which its amount is suspected to be far beyond its saturation solubility. The reducibility of the updoped LSCF was found to be much better than that of the undoped CZO, evidenced by the H_2-TPR of the both materials at 600 °C where the oxygen storage capacity of LSCF and CZO was determined at 4273 and 307 $\mu mol/g_{cat}$, respectively. In contrast, the oxygen storage capacity of 40%Ni-CZO (where x = 0.7, 0.9) was found to be higher than that of the LSCF, implying that the addition of Ni caused more electronic defect and enhanced the oxygen mobility in CZO than in LSCF, according to the H_2-TPR results. Coke resistant of CZO is presumable more satisfying than that of LSCF, thus, the longer lifespan of the CZO catalyst system is expected. The catalytic performance of 40%Ni-CZO (x = 0.9) was however comparable with 40%Ni-LSCF as they accommodate the same number of active sites and the oxygen storage capacity was not as much involved. However, the slightly better catalytic performance of the 40%Ni-CZO (x = 0.9) could be due to its smaller crystallite size (CZO = 26.83, LSCF = 35.73), rendering easier access for the relevant gaseous reactants.

Credit author statement

Chalempol Khajonvittayakul: Writing – original draft, Investigation **Vut Tongnan**: Investigation, experimenting, Visualization, Data curation, Methodology. **Netiwat namo**: Visualization, Data curation. **Chutamat Phonbubpha** Visualization, Data curation. **Navadol Laosiripojana**: Formal analysis **Suksun amornraksa**,: Interpretation, Supervision, writing, editing **Matthew Hartley**: Resources, Validation **U.W. Hartley**: Supervision, Writing – review & editing, Conceptualization, Funding acquisition

Declaration of competing interest

The authors declare that they have no known competing financial interests or personal relationships that could have appeared to influence the work reported in this paper.

Acknowledgements

This work was supported by Thailand Research Fund (RSA6180061), King Mongkut's University of Technology North Bangkok (KMUTNB-BasicR-64-31, KMUTNB-BasicR-64-34 and KMUTNB-PHD-62-10).

References

Alvarez-Galvan, C., Melian, M., Ruiz-Matas, L., Eslava, J.L., Navarro, R.M., Ahmadi, M., Cuenya, B.R., Fierro, J.L.G., 2019. Partial oxidation of methane to syngas over nickel-based catalysts: influence of support type, addition of rhodium, and preparation method. Front. Chem. 7, 1–16. https://doi.org/10.3389/fchem.2019.00104.

Ashok, J., Kawi, S., 2013. Steam reforming of toluene as a biomass tar model compound over CeO 2 promoted Ni/CaOeAl2O3 catalytic systems. Int. J. Hydrogen Energy 38, 13938–13949. https://doi.org/10.1016/j.ijhydene.2013.08.029.

Ashok, J., Kathiraser, Y., Ang, M.L., Kawi, S., 2015. Bi-functional hydrotalcite-derived NiO-CaO-Al2O3 catalysts for steam reforming of biomass and/or tar model compound at low steam-to-carbon conditions. Appl. Catal. B Environ. 172, 116–128. https://doi.org/10.1016/j.apcatb.2015.02.017.

Ashok, J., Ang, M.L., Kawi, S., 2017. Enhanced activity of CO2 methanation over Ni/CeO2-ZrO2 catalysts: influence of preparation methods. Catal. Today 281, 304–311. https://doi.org/10.1016/j.cattod.2016.07.020.

Babiniec, S.M., Coker, E.N., Miller, J.E., Ambrosini, A., 2015. Investigation of La Sr1−Co M1−O3− (M = Mn, Fe) perovskite materials as thermochemical energy storage media. Sol. Energy 118, 451–459. https://doi.org/10.1016/j.solener.2015.05.040.

Bai, 2013. The Microemulsion Preparation and High Catalytic Performance of Mesoporous NiO Nanorods and Nanocubes for Toluene Combustion. https://doi.org/10.1016/j.cej.2013.01.008.

Baker, E.G., Mudge, L.K., Brown, M.D., 1987. Steam gasification of biomass with nickel secondary catalysts. Ind. Eng. Chem. Res. 26, 1335–1339. https://doi.org/10.1021/ie00067a012.

Bampenrat, A., Meeyoo, V., Kitiyanan, B., Rangsunvigit, P., Rirksomboon, T., 2010. Naphthalene steam reforming over Mn-doped CeO2-ZrO2 supported nickel catalysts. Appl. Catal. A Gen. 373, 154–159. https://doi.org/10.1016/j.apcata.2009.11.008.

Biswas, P., Kunzru, D., 2007. Steam reforming of ethanol for production of hydrogen over Ni/CeO2-ZrO2 catalyst: effect of support and metal loading. Int. J. Hydrogen Energy 32, 969–980. https://doi.org/10.1016/j.ijhydene.2006.09.031.

Chen, J., Wu, Q., Zhang, Jianxiang, Zhang, Jiyan, 2008. Effect of preparation methods on structure and performance of Ni/Ce0.75Zr0.25O2 catalysts for CH4-CO2 reforming. Fuel 87, 2901–2907. https://doi.org/10.1016/j.fuel.2008.04.015.

Córdoba, L.F., Martínez-Hernández, A., 2015. Preferential oxidation of CO in excess of hydrogen over Au/CeO2-ZrO2 catalysts. Int. J. Hydrogen Energy 40, 16192–16201. https://doi.org/10.1016/j.ijhydene.2015.09.133.

Dayton, D., 2002. Review of the Literature on Catalytic Biomass Tar Destruction: Milestone Completion Report. National Renewable Energy Laboratory, Golden, CO. https://doi.org/10.2172/15002876.

Ding, X., Liu, Y., Gao, L., Guo, L., 2008. Synthesis and characterization of doped LaCrO3 perovskite prepared by EDTA-citrate complexing method. J. Alloys Compd. 458, 346–350. https://doi.org/10.1016/j.jallcom.2007.03.110.

Gao, N., Liu, S., Han, Y., Xing, C., Li, A., 2015. Steam reforming of biomass tar for hydrogen production over NiO/ceramic foam catalyst. Int. J. Hydrogen Energy 40, 7983–7990. https://doi.org/10.1016/j.ijhydene.2015.04.050.

Garcia, L., French, R., Czernik, S., Chornet, E., 2000. Catalytic steam reforming of bio-oils for the production of hydrogen: effects of catalyst composition. Appl. Catal. A Gen. 201, 225–239. https://doi.org/10.1016/S0926-860X(00)00440-3.

Guan, G., Kaewpanha, M., Hao, X., Abudula, A., 2016. Catalytic steam reforming of biomass tar: prospects and challenges. Renew. Sustain. Energy Rev. 58, 450–461. https://doi.org/10.1016/j.rser.2015.12.316.

Han, J., Kim, H., 2008. The reduction and control technology of tar during biomass gasification/pyrolysis: an overview. Renew. Sustain. Energy Rev. 12, 397–416. https://doi.org/10.1016/j.rser.2006.07.015.

Hartley, U.W., Amornraksa, S., Kim-Lohsoontorn, P., Laosiripojana, N., 2015. Thermodynamic analysis and experimental study of hydrogen production from oxidative reforming of n-butanol. Chem. Eng. J. 278, 2–12. https://doi.org/10.1016/j.cej.2015.02.016.

Hartley, U.W., Tongnan, V., Laosiripojana, N., Kim-Lohsoontorn, P., Li, K., 2018. Nitrous oxide decomposition over La0.3Sr0.7Co0.7Fe0.3O3−δ catalyst. React. Kinet. Mech. Catal. 125, 85–97. https://doi.org/10.1007/s11144-018-1398-9.

Hernández, S., Farkhondehfal, M.A., Sastre, F., Makkee, M., Saracco, G., Russo, N., 2017. Syngas production from electrochemical reduction of CO2: current status and prospective implementation. Green Chem. 19, 2326–2346. https://doi.org/10.1039/c7gc00398f.

Higo, T., Hashimoto, T., Mukai, D., Nagatake, S., Ogo, S., Sugiura, Y., Sekine, Y., 2015. Effect of hydrocarbon structure on steam reforming over Ni/perovskite catalyst. J. Japan Pet. Inst. 58, 86–96. https://doi.org/10.1627/jpi.58.86.

Jang, W.J., Shim, J.O., Kim, H.M., Yoo, S.Y., Roh, H.S., 2019. A review on dry reforming of methane in aspect of catalytic properties. Catal. Today 15–26. https://doi.org/10.1016/j.cattod.2018.07.032.

Kangsadan, T., Srisurat, T., Kim, P., Laosiripojana, N., Jindasuwan, S., Hartley, U.W., 2015. Hydrogen production from palmitic acid through autothermal reforming: thermodynamic analysis. Eng. J. 19, 153–165. https://doi.org/10.4186/ej.2015.19.4.153.

Khajonvittayakul, C., Tongnan, V., Kangsadan, T., Laosiripojana, N., Jindasuwan, S., Hartley, U.W., 2019. Thermodynamic and mechanism study of syngas production via integration of nitrous oxide decomposition and methane partial oxidation in the presence of 10%NiO–La0.3Sr0.7Co0.7Fe0.3O3−Δ. React. Kinet. Mech. Catal. 127, 839–855. https://doi.org/10.1007/s11144-019-01600-1.

Khamhangdatepon, T., Tongnan, V., Hartley, M., Sornchamni, T., Siri-Nguan, N., Laosiripojana, N., Li, K., Hartley, U.W., 2020. Mechanisms of synthesis gas production via thermochemical cycles over La0·3Sr0·7Co0·7Fe0·3O3. Int. J. Hydrogen Energy. https://doi.org/10.1016/j.ijhydene.2019.12.148.

Kuchonthara, P., Puttasawat, B., Piumsomboon, P., Mekasut, L., Vitidsant, T., 2012. Catalytic steam reforming of biomass-derived tar for hydrogen production with K 2CO 3/NiO/γ-Al 2O 3 catalyst. Kor. J. Chem. Eng. https://doi.org/10.1007/s11814-012-0027-y.

Laosiripojana, N., Assabumrungrat, S., 2005. Methane steam reforming over Ni/Ce-ZrO2 catalyst: influences of Ce-ZrO2 support on reactivity, resistance toward carbon formation, and intrinsic reaction kinetics. Appl. Catal. A Gen. 290, 200–211. https://doi.org/10.1016/j.apcata.2005.05.026.

Laosiripojana, N., Assabumrungrat, S., 2006. Catalytic steam reforming of ethanol over high surface area CeO2: the role of CeO2 as an internal pre-reforming

catalyst. Appl. Catal. B Environ. 66, 29–39. https://doi.org/10.1016/j.apcatb.2006.01.011.
Li, 2019. NiCo@NiCo Phyllosilicate@CeO2 Hollow Core Shell Catalysts for Steam Reforming of Toluene as Biomass Tar Model Compound. https://doi.org/10.1016/j.enconman.2018.11.034.
Li, C., Hirabayashi, D., Suzuki, K., 2009a. Development of new nickel based catalyst for biomass tar steam reforming producing H2-rich syngas. Fuel Process. Technol. 90, 790–796. https://doi.org/10.1016/j.fuproc.2009.02.007.
Li, C., Hirabayashi, D., Suzuki, K., 2009b. A crucial role of O2− and O22− on mayenite structure for biomass tar steam reforming over Ni/Ca12Al14O33. Appl. Catal. B Environ. 88, 351–360. https://doi.org/10.1016/j.apcatb.2008.11.004.
Li, W., Liu, H., Chen, Y., 2017. Promotion of transition metal oxides on the NH3-SCR performance of ZrO2-CeO2 catalyst. Front. Environ. Sci. Eng. 11, 6. https://doi.org/10.1007/s11783-017-0914-x.
Liu, 2018. Oxygen Vacancy Promoting Dimethyl Carbonate Synthesis from CO2 and Methanol over Zr-Doped CeO2 Nanorods. https://doi.org/10.1021/acscatal.8b00415.
Liu, C., Chen, D., Cao, Y., zhang, T., Mao, Y., Wang, W., Wang, Z., Kawi, S., 2020a. Catalytic steam reforming of in-situ tar from rice husk over MCM-41 supported LaNiO3 to produce hydrogen rich syngas. Renew. Energy 161, 408–418. https://doi.org/10.1016/j.renene.2020.07.089.
Liu, Y., Song, J., Diao, X., Liu, L., Sun, Y., 2020b. Removal of tar derived from biomass gasification via synergy of non-thermal plasma and catalysis. Sci. Total Environ. 721, 137671. https://doi.org/10.1016/j.scitotenv.2020.137671.
Milne, T.A., Evans, R.J., Abatzaglou, N., 1998. Biomass Gasifier "'Tars'": Their Nature, Formation, and Conversion, Developments in Thermochemical Biomass Conversion. Golden, CO, (United States). https://doi.org/10.2172/3726.
Monshi, A., Foroughi, M.R., Monshi, M.R., 2012. Modified scherrer equation to estimate more accurately nano-crystallite size using XRD, 02 World J. Nano Sci. Eng. 154–160. https://doi.org/10.4236/wjnse.2012.23020.
Mukai, D., Tochiya, S., Murai, Y., Imori, M., Hashimoto, T., Sugiura, Y., Sekine, Y., 2013. Role of support lattice oxygen on steam reforming of toluene for hydrogen production over Ni/La0.7Sr0.3AlO3-δ catalyst. Appl. Catal. A Gen. https://doi.org/10.1016/j.apcata.2012.11.040.
Nakamura, S., Kitano, S., Yoshikawa, K., 2016. Biomass gasification process with the tar removal technologies utilizing bio-oil scrubber and char bed. Appl. Energy 170, 186–192. https://doi.org/10.1016/j.apenergy.2016.02.113.
Nam, H., Wang, Z., Shanmugam, S.R., Adhikari, S., Abdoulmoumine, N., 2018. Chemical looping dry reforming of benzene as a gasification tar model compound with Ni- and Fe-based oxygen carriers in a fluidized bed reactor. Int. J. Hydrogen Energy 43, 18790–18800. https://doi.org/10.1016/j.ijhydene.2018.08.103.
Ngoenthong, N., Hartley, M., Sornchamni, T., Siri-nguan, N., Laosiripojana, N., Hartley, U.W., 2019. Comparison of packed-bed and micro-channel reactors for hydrogen production via thermochemical cycles of water splitting in the presence of ceria-based catalysts. Processes 7, 1–12. https://doi.org/10.3390/pr7100767.
Nie, W., Zou, X., Chen, C., Wang, X., Ding, W., Lu, X., 2017. Methanation of carbon dioxide over Ni–Ce–Zr oxides prepared by one-pot hydrolysis of metal nitrates with ammonium carbonate. Catalysts 7, 104. https://doi.org/10.3390/catal7040104.
Oemar, 2014. Mechanism and kinetic modeling for steam reforming of toluene on La0.8Sr0.2Ni0.8Fe0.2O3 catalyst. AIChE J. https://doi.org/10.1002/aic.14573.
Oemar, 2015. Role of lattice oxygen in oxidative steam reforming of toluene as a tar model compound over Ni/La 0.8 Sr 0.2 AlO 3 catalyst. Catal. Sci. Technol. https://doi.org/10.1039/C5CY00412H.
Pengpanich, S., Meeyoo, V., Rirksomboon, T., 2004. Methane partial oxidation over Ni/CeO2-ZrO2 mixed oxide solid solution catalysts. Catal. Today 93 (95), 95–105. https://doi.org/10.1016/j.cattod.2004.06.079.
Sekine, Y., Mukai, D., Murai, Y., Tochiya, S., Izutsu, Y., Sekiguchi, K., Hosomura, N., Arai, H., Kikuchi, E., Sugiura, Y., 2013. Steam reforming of toluene over perovskite-supported Ni catalysts. Appl. Catal. A Gen. 451, 160–167. https://doi.org/10.1016/j.apcata.2012.11.005.
Soomro, A., Chen, S., Ma, S., Xiang, W., 2018. Catalytic activities of nickel, dolomite, and olivine for tar removal and H2-enriched gas production in biomass gasification process. Energy Environ. 29, 839–867. https://doi.org/10.1177/0958305X18767848.
Sordi, A., Da Silva, E.P., Neto, A.J.M., Lopes, D.G., Pinto, C.S., Araújo, P.D., 2009. Thermodynamic simulation of biomass gas steam reforming for a solid oxide fuel cell (SOFC) system. Braz. J. Chem. Eng. 26, 745–755. https://doi.org/10.1590/S0104-66322009000400013.
Sun, F.M., Yan, C.F., Wang, Z. Da, Guo, C.Q., Huang, S.L., 2015. Ni/Ce-Zr-O catalyst for high CO2 conversion during reverse water gas shift reaction (RWGS). Int. J. Hydrogen Energy 40, 15985–15993. https://doi.org/10.1016/j.ijhydene.2015.10.004.
Sun, L., Cao, S., Huang, Y., Zhang, Y., Xiao, Y., Dong, G., Su, Y., 2019. VOX supported on TiO2-Ce0.9Zr0.1O2 core-shell structure catalyst for NH3-SCR of NO. RSC Adv. 9, 30340–30349. https://doi.org/10.1039/c9ra05024h.
Świerczyński, D., Libs, S., Courson, C., Kiennemann, A., 2007. Steam reforming of tar from a biomass gasification process over Ni/olivine catalyst using toluene as a model compound. Appl. Catal. B Environ. 74, 211–222. https://doi.org/10.1016/j.apcatb.2007.01.017.
Trovarelli, A., Zamar, F., Llorca, J., De Leitenburg, C., Dolcetti, G., Kiss, J.T., 1997. Nanophase fluorite-structured CeO2-ZrO2 catalysts prepared by high-energy mechanical milling: analysis of low-temperature redox activity and oxygen storage capacity. J. Catal. 169, 490–502. https://doi.org/10.1006/jcat.1997.1705.
Urasaki, K., Sekine, Y., Kawabe, S., Kikuchi, E., Matsukata, M., 2005. Catalytic activities and coking resistance of Ni/perovskites in steam reforming of methane. Appl. Catal. A Gen. 286, 23–29. https://doi.org/10.1016/j.apcata.2005.02.020.
Vivanpatarakij, S., Assabumrungrat, S., 2013. Thermodynamic analysis of combined unit of biomass gasifier and tar steam reformer for hydrogen production and tar removal. Int. J. Hydrogen Energy 38, 3930–3936. https://doi.org/10.1016/j.ijhydene.2012.12.039.
Wetwatana, U., Kim-Lohsoontorn, P., Assabumrungrat, S., Laosiripojana, N., 2010. Catalytic steam and autothermal reforming of used lubricating oil (ULO) over Rh- and Ni-based catalysts. Ind. Eng. Chem. Res. 49, 10981–10985. https://doi.org/10.1021/ie1004288.
Zhang, 2019. Fuel. https://doi.org/10.1016/j.fuel.2019.116032.
Zhao, B., Zhang, X., Chen, L., Qu, R., Meng, G., Yi, X., Sun, L., 2010. Steam reforming of toluene as model compound of biomass pyrolysis tar for hydrogen. Biomass Bioenergy 34, 140–144. https://doi.org/10.1016/j.biombioe.2009.10.011.
Łamacz, A., Krztoń, A., Djéga-Mariadassou, G., 2011. Steam reforming of model gasification tars compounds on nickel based ceria-zirconia catalysts. Catal. Today 176, 347–351. https://doi.org/10.1016/j.cattod.2010.11.067.
Łamacz, A., Babiński, P., Łabojko, G., 2019. The impact of components of synthesis gas from coal gasification on conversion of model tar compounds over Ni/CeZrO2 catalyst. Fuel 236, 984–992. https://doi.org/10.1016/j.fuel.2018.09.075.